A NUMERICAL INVESTIGATION OF THE INFLUENCE OF BAFFLE CURVATURE ON THE HYDRODYNAMIC PERFORMANCE OF A NON-NEWTONIAN FLUID IN A SPHERICAL STIRRED VESSEL EQUIPPED WITH A RADIAL IMPELLER

Abderrahim Sidi Mohammed NEKROUF [1], Sarra YOUCEFI [2,*], Abderrahim MOKHEFI [3], Houssem LAIDOUDI [4]

Agitation in spherical tanks enhances mixing efficiency and fluid property control in various industrial processes. This study presents a numerical investigation of the influence of curved baffles installed on the wall of a spherical vessel stirred by a disk turbine and filled with a non-Newtonian fluid. The impact of baffle orientation (vertical or horizontal), number ($4 \leq b \leq 10$), flow behavior index ($0.6 \leq n \leq 1.4$), and Reynolds number ($1 \leq Re \leq 150$) on the hydrodynamics and energy consumption is analyzed. The laminar flow equations are solved under steady-state using the finite volume method. The results have demonstrated that the installation of horizontal baffles in spherical vessels with a radial turbine is beneficial in terms of enhancing radial flow. Furthermore, increasing their number improves axial flow intensity. However, although power tends to increase with the installation of such baffles, the percentage of increase only reaches 0.86% at moderate rotational speeds for 10 baffles.

Keywords: Stirred vessel, numerical modeling, non-Newtonian fluid, hydrodynamics, baffle.

1. Introduction

Mechanical agitation is widely used in industries such as chemical, pharmaceutical, polymer, and wastewater treatment. Mixing efficiency depends on hydrodynamic flow conditions and the mixture's physicochemical properties. Key factors include uniform velocity distribution, absence of stagnant zones,

[1] PhD., Laboratory of Applied Mechanics, Department of Mechanical Engineering, University of Science and Technology of Oran MB, Algeria, abderrahimmohammed.nekrouf@univ-usto.dz
[2] Prof., Department of Mechanical Engineering, University of Science and Technology of Oran MB, Algeria, sarra.youcefi@univ-usto.dz
[3] Associated Prof., LTE Laboratory, Mechanical Department, National Polytechnic School of Oran, Algeria, abderahimmokhefi@yahoo.fr
[4] Associated Prof., Laboratory of Sciences and Marine Engineering, Department of Marine Engineering, University of Science and Technology of Oran MB, Algeria, hichemsoft19@gmail.com

efficient energy dissipation, and well-defined circulation patterns. Common agitation tanks include flat-bottomed, dished-bottomed, conical, and spherical designs, tailored to specific applications. [1-3]

Given the importance of agitation, research has focused on enhancing the hydrodynamic and energy performance of stirred tanks through modifications to impeller designs or tank geometry. Ameur [4] showed numerically that spherical tanks equipped with a Scaba agitator provide uniform flow with lower energy consumption compared to other shapes. Tacă and Păunescu [5] found that spherical tanks agitated by Rushton or inclined turbines are up to 30% more energy-efficient than cylindrical tanks. Yapici and Basturk [6] analyzed heat transfer in hemispherical stirred vessels, observing periodic temperature decreases under controlled heating.

Impeller turbines are widely used in agitation systems to enhance gas or liquid exchange, dispersion, mixing, and homogenization. Researchers have explored various design modifications, including blade inclination and the addition of baffles and slots. Distelhoff et al. [7] showed that inclined blades localize concentration above and below Rushton turbines. Chapple et al. [8] found that inclined blades reduce energy consumption compared to standard designs. Aubin et al. [9] observed minimal changes in liquid flow patterns in aerated tanks agitated by inclined blade turbines. The Pitched Blade Turbine Up-Pumping (PBTU) configuration was shown to entrain 36% more gas compared to the Pitched Blade Turbine Down-Pumping (PBTD) configuration. Boonkanokwong et al. [10] demonstrated that torque in cylindrical blade turbines depends on blade count. Overall, significant modifications to impellers and tanks have improved hydrodynamics, energy efficiency, and performance in both turbulent and laminar flows [2,11-14].

The use of baffles reduces vortex size and enhances top-to-bottom circulation, decreasing mixing time but significantly increasing power consumption. Numerical and experimental studies have explored baffle effects in agitated tanks. Zadghaffari et al. [15] studied baffled tanks stirred by Rushton turbines, observing reduced mixing time and increased stirring power. Xiong et al. [16] compared configurations with and without baffles, finding baffles with holes to be more efficient. Youcefi et al. [17,18] analyzed baffled, unbaffled, and slotted tanks, noting that slot placement reduced vortex size and energy use. Roy et al. [19] used LES simulation to study inclined blades in baffled tanks, finding an 18% higher power input under perturbation, optimizing energy for faster mixing.

Non-Newtonian fluids, whose viscosity varies with shear stress, are widely used in industry. Studies such as those by Youcefi and Youcefi [20] highlight the strong dependence of mixing time on fluid elasticity in tanks with two-blade impellers. Tanguy and Ascanio [21] found that agitator position significantly affects mixing times for shear-thinning fluids. Recent research further explores

the complex behaviors of non-Newtonian fluids in agitated tanks [22-27]. Based on the analysis of literature, it appears that despite the significance of spherical tanks in industrial applications, limited studies have been conducted on the hydrodynamic, energetic, and even thermal behaviors of such mechanically agitated tank configurations investigation into the implementation of spherical agitated tanks equipped with a disk turbine and filled with a shear-thinning fluid. The aim is to highlight the influence of baffles, impeller rotational speed, and fluid complexity on the conventional performance of mechanical agitation. This study presents interesting conclusions aimed at improving the design of these systems, given their quasi absence in various applications.

2. Description of mixing system

The agitation system consists of a spherical vessel of diameter *D*. This vessel is equipped with a disk turbine impeller of diameter *d* attached to a disk of diameter *w* and thickness *t*. The clearance between the bottom of the vessel and the mid-section of the turbine disk is *C*. The length and width of the blades respectively are *L* and *h*. The disk is mounted on a cylindrical central shaft of diameter *ds*, see Figure 1.

The geometrical ratios used to concept the present agitation system are shown in Table 1.

The agitated vessel is filled with a non-Newtonian fluid with a density of 1394 kg/m^3, a flow consistency index of 8 Pa s^n and a flow behavior index [23]. For flow indices below 1, the fluid is classified as pseudoplastic, characterized by a decrease in viscosity as the shear rate increases, facilitating flow under shear. In contrast, fluids with indices above 1 are shear-thickening, where viscosity increases with shear rate.

Table 1

Details of all geometrical configurations simulated

D[mm]	d/D	C/D	w/D	t/D	LD	h/D	ds/D	a/D	e/D
300	0.5	0.5	0.06	0.01	0.221	0.066	0.05	0.1	0.003

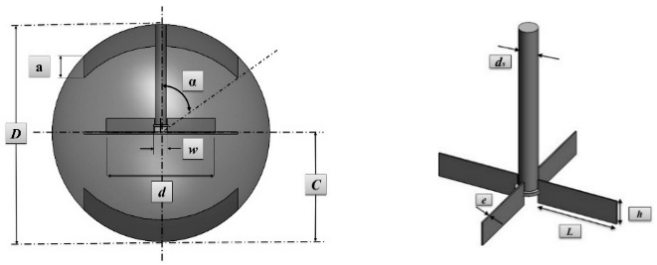

Fig. 1. Spherical vessel equipped with a disk turbine impeller

Our study focused on these fluids, selected for their energy efficiency and enhanced mixing under shear. Three configurations were tested based on the installation of curved baffles: no baffles, vertical baffles, and horizontal baffles (Figure 2). Additionally, a comparative analysis was conducted using four different baffle quantities: 4, 6, 8, and 10 (Figures 2 and 3).

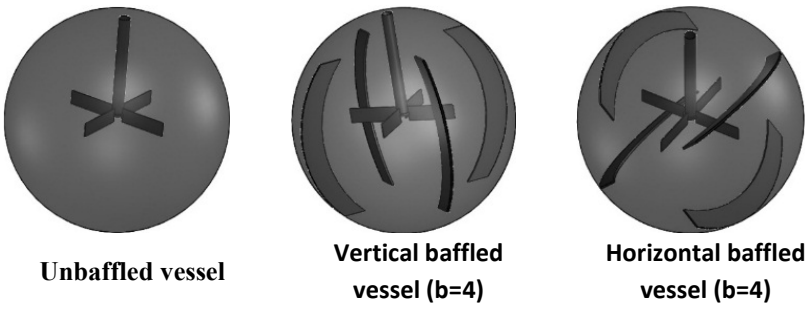

Fig. 2. Different design of spherical stirred vessels according to baffle installation

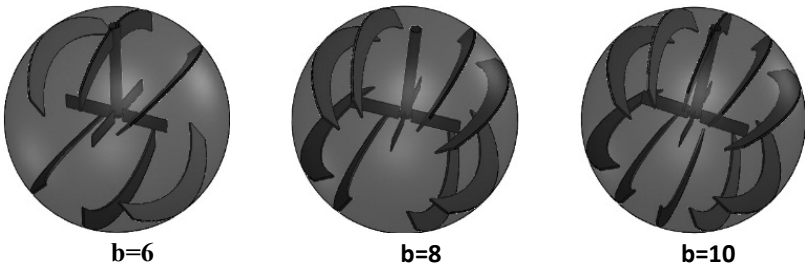

Fig. 3. Different design of spherical stirred vessels according to baffle number

3. Mathematical model

The flow generated by mechanical agitation in the spherical vessel is governed by the continuity and momentum conservation equations. Assuming a purely laminar stationary regime and using a Cartesian coordinate system (*OXYZ*), the governing equations for a non-Newtonian fluid are as follows:

Mass balance

$$\frac{\partial U}{\partial X}+\frac{\partial V}{\partial Y}+\frac{\partial W}{\partial Z}=0 \tag{1}$$

Momentum balance

$$\rho\left(U\frac{\partial U}{\partial X}+V\frac{\partial U}{\partial Y}+W\frac{\partial U}{\partial Z}\right)=-\frac{\partial P}{\partial X}+\frac{\partial \tau_{XX}}{\partial X}+\frac{\partial \tau_{XY}}{\partial Y}+\frac{\partial \tau_{XZ}}{\partial Z} \tag{2}$$

$$\rho\left(U\frac{\partial V}{\partial X}+V\frac{\partial V}{\partial Y}+W\frac{\partial V}{\partial Z}\right)=-\frac{\partial P}{\partial Y}+\frac{\partial \tau_{XY}}{\partial X}+\frac{\partial \tau_{YY}}{\partial Y}+\frac{\partial \tau_{YZ}}{\partial Z} \tag{3}$$

$$\rho\left(U\frac{\partial W}{\partial X}+V\frac{\partial W}{\partial Y}+W\frac{\partial W}{\partial Z}\right)=-\frac{\partial P}{\partial Z}+\frac{\partial \tau_{XZ}}{\partial X}+\frac{\partial \tau_{YZ}}{\partial Y}+\frac{\partial \tau_{ZZ}}{\partial Z}-\rho g \tag{4}$$

With (U, V, W) and P present respectively the velocity field and pressure the fluid. τ presents the shear stress, defined as:

$$\tau_{ij}=2\eta\varepsilon_{ij}, \tag{5}$$

In this equation,τ_{ij} and ε_{ij} represent the viscous stress and deformation rate tensors, respectively, while η denotes the apparent dynamic viscosity, which depends on the flow consistency index m and the flow behavior index n. The viscosity η is calculated as follows [26]:

$$\eta=m\dot{\gamma}^{n-1}, \tag{6}$$

With $\dot{\gamma}$ representing the velocity gradient, defined by [26]:

$$\dot{\gamma}=\sqrt{2\left[\left(\frac{\partial U}{\partial X}\right)^2+\left(\frac{\partial V}{\partial Y}\right)^2+\left(\frac{\partial W}{\partial Z}\right)^2\right]+\left(\frac{\partial U}{\partial Y}+\frac{\partial V}{\partial X}\right)^2+\left(\frac{\partial U}{\partial Z}+\frac{\partial W}{\partial X}\right)^2+\left(\frac{\partial V}{\partial Z}+\frac{\partial W}{\partial Y}\right)^2} \tag{7}$$

For non-Newtonian fluids, the Reynolds number (Re) is a function of the flow behavior index n and the rotational speed N. For n = 0.8 and Re from 1 to 150, N ranges from 0.32 to 20.84 *rps* (*Revolutions Per Second*). The Reynolds number is defined as follows:

$$\mathrm{Re}=\frac{\rho N^{2-n}d^2}{m} \tag{8}$$

The impeller diameter is used to express the Reynolds number to represent the direct influence of geometry on agitation performance due to the MRF approach.

We used the Moving Reference Frame (MRF) technique to simplify rotational effects by making the impeller stationary within the moving reference frame, also known as the 'Frozen Rotor' approach. The Navier-Stokes equations are solved in this frame for rotating regions and in a fixed frame for stationary zones, ensuring continuity between domains. This method reduces computation time by treating rotation as an imposed condition, maintaining precision while enabling detailed flow analysis. It also simplifies modeling for non-cylindrical geometries by reformulating equations in the moving frame. In accordance with commonly adopted practices in the literature, only the impeller and the lower part of the shaft are included in the rotating domain. Although the entire shaft is theoretically rotating, this simplification reduces the complexity of the model

while maintaining adequate kinematic consistency. This approach is widely used in studies dealing with modeling by the MRF method [17-18,28-30].

As the tangential, radial and axial velocities are commonly used in the interpretation of such agitation system, they are hence employed in the present study. From the Cartesian Velocities U, V and W, the tangential and radial, axial velocities are thus given by:

$$V_\theta = \frac{-UY + VX}{\sqrt{X^2 + Y^2}}, \quad V_r = \frac{UX + VY}{\sqrt{X^2 + Y^2}}, \quad V_Z = W \tag{9}$$

To analyze the theoretical results, velocity components and spatial coordinates (radial R and axial Z) are converted to dimensionless form using the following equations:

$$(V_\theta^*, V_r^*, V_Z^*) = \frac{(V_\theta, V_r, V_Z)}{\pi ND}, \quad R^* = \frac{2R}{D}, \quad Z^* = \frac{2Z}{D} \tag{10}$$

The power consumption of the agitation system can be determined from CFD data. It is derived from fluid shear resistance, reflecting the friction within the agitated liquid. Based on the viscous dissipation function, this power, denoted as Po is calculated by:

$$Po = \iiint_{\text{Vessel volume}} \eta Q_v \, \mathrm{d}X \, \mathrm{d}Y \, \mathrm{d}Z \tag{11}$$

In this context, Qv represents the viscous dissipation function, which is determined by the following formula:

$$Q_v = 2\left[\left(\frac{\partial U}{\partial X}\right)^2 + \left(\frac{\partial V}{\partial Y}\right)^2 + \left(\frac{\partial W}{\partial Z}\right)^2\right] + \left(\frac{\partial U}{\partial Y} + \frac{\partial V}{\partial X}\right)^2 + \left(\frac{\partial U}{\partial Z} + \frac{\partial W}{\partial X}\right)^2 + \left(\frac{\partial V}{\partial Z} + \frac{\partial W}{\partial Y}\right)^2 \tag{12}$$

The power number, a dimensionless indicator of consumed power, provides key insights into the stirred system and is calculated using the following expression:

$$N_P = \frac{Po}{\rho N^3 d^5} \tag{13}$$

Table 2

Boundary conditions

Boundary	**Conditions**
Disk turbine walls	$V_\theta = \pi Nr$, $V_r = 0$ and $V_z = 0$
Spherical vessel wall	$V_\theta = V_r = V_z = 0$

The boundary conditions are critical for accurately modeling fluid flow. Key conditions include the rotational velocity at the impeller wall, where the impeller rotates at a constant speed to drive fluid movement, and the non-slip

condition at the vessel wall, ensuring zero fluid velocity relative to the wall. These conditions simulate realistic fluid dynamics, enabling insights into the interplay between the rotating impeller and stationary walls. Table 2 lists the simulation parameters.

4. Numerical methods

4.1 Numerical detail

The present study employs CFD to solve the Navier-Stokes equations for incompressible shear-thinning fluids in the 3D flow field generated by a disk turbine. Using the finite volumes method, partial differential equations representing conservation laws are transformed into discrete algebraic equations. These equations are solved to determine the dependent variable values for each volume. For details, see Moukalled et al. [31]. A purely tetrahedral mesh was utilized, refined at critical areas such as impeller boundaries, vessel walls, and baffles (Figure 4a). A five-layer prismatic mesh near fixed walls (Figure 4b) enhances boundary layer resolution, capturing velocity gradients effectively. The optimal mesh includes 150,393 nodes and 740,650 elements (681,115 tetrahedral, 59,535 prisms), ensuring geometric precision and computational efficiency. To simulate the irregular rotational motion of the disk turbine, relative motion is applied by defining a rotating cylindrical domain around the turbine. This creates a mobile rotating domain and a stationary residual domain. Tangential velocities at the cylindrical boundary account for relative motion, accelerations, and the Coriolis effect, ensuring accurate flow dynamics modeling.

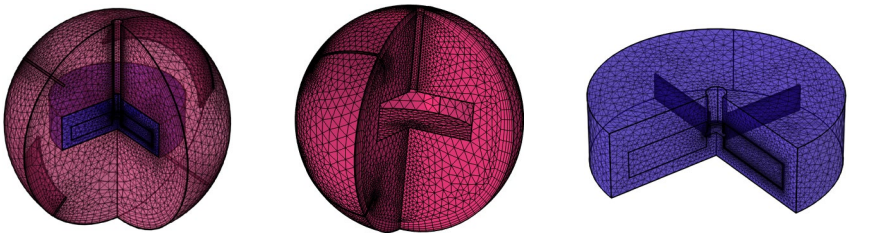

Fig. 4. Studied computational domain mesh

4.2 MESH CHECK

To ensure the independence of the numerical results from the mesh structure, a mesh sensitivity test was performed using progressively refined meshes, as shown in Table 3. Three meshes (M1-M3) were tested to verify the

validity of the results. The data shows the number of elements and the evolution of power number values (N_p). The M2 mesh, containing 740,650 tetrahedral elements, was selected as the power number values remained virtually unchanged. The results were considered convergent when the residue reached 10^{-6} and field values remained nearly identical over the last 1000 iterations

Table 3

Variation of power number with number of elements at Re = 10

Mesh	**M1**	**M2**	**M3**
Elements	247514	740650	1089353
Power number	3.6928	3.9541	3.9572

4.3 Code validation

In order to prove the numerical reliability of the simulations and the consistency of the results, it is important to validate the numerical methods used before the investigation. To guarantee the similarity of numerical results, we refer to the study by Ameur [23] using the same simulation conditions. We have highlighted a global and local characteristic of great importance, respectively the power number and tangential velocity, for a wide range of Reynolds number, as shown in Figure 5. Comparison of the predicted results with numerical data from Ameur [23] shows good agreement.

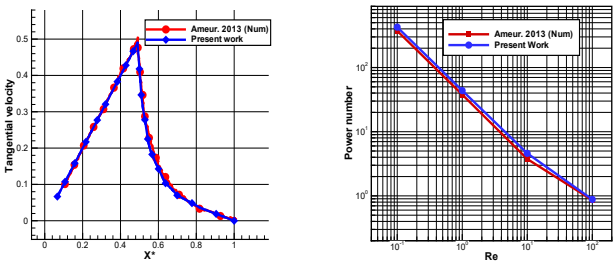

Fig. 5. Comparison of the results obtained from the current code with those of reference

5. Results and discussions

This section presents the results of the numerical simulation of laminar flow of a shear-thinning fluid in a spherical vessel equipped with a disk turbine. The effects of Reynolds number, baffle shape, number of baffles, and behavior index on hydrodynamics and energy are analyzed. The results include velocity contours and streamlines in the impeller and horizontal planes, along with graphs of tangential and radial velocity components along horizontal lines.

Additionally, the axial velocity distribution is shown along vertical lines, as illustrated in Figures 6.

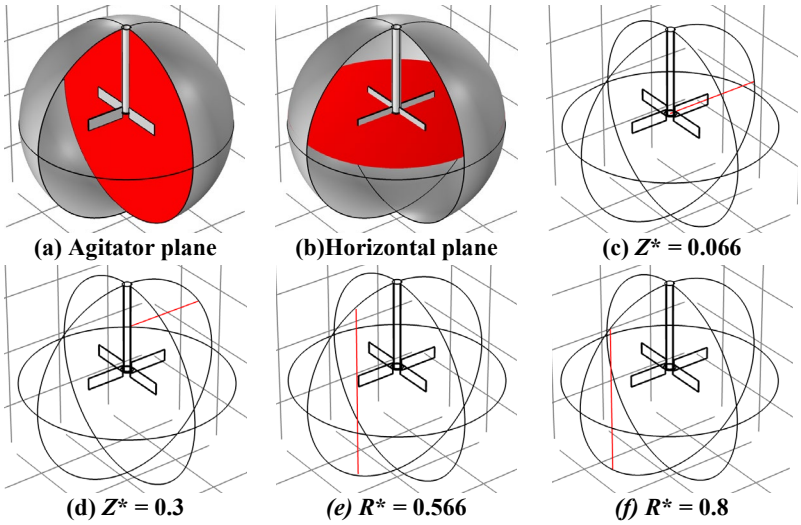

Fig. 6. Measurement planes and lines

5.1 Effect of vessel configuration

In this subsection, the hydrodynamics of the vessel's shape, characterized by the presence of four baffles arranged in different configurations, are examined. To accomplish this, Reynolds number has been set to its maximum value of 150, considering a shear-thinning fluid with an index of 0.8.

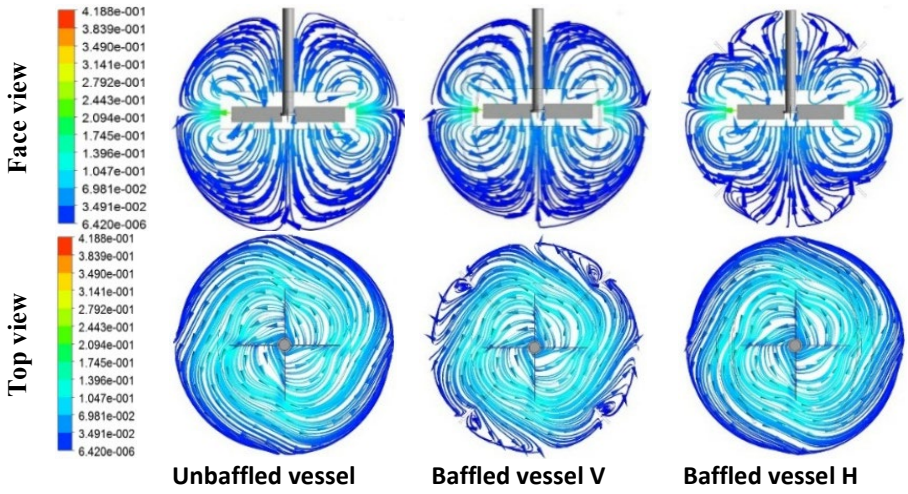

Fig. 7. Streamlines for different vessel shapes according to different views

The configuration of streamline patterns for different designs of the spherical vessel is presented in Figure 7 across the entire domain as well as on the two measurement planes (Figure 6). At the vertical plane, the introduction of vertical baffles does not lead to a pronounced alteration in the flow structure. However, the presence of horizontal baffles contributes to the generation of additional axial flow loops at the top and bottom of the spherical vessel. This is due to the disruption of axial flow caused by the horizontal obstacles, resulting in the formation of additional axial loops. On the horizontal plane, the influence of vertical baffles is depicted on the tangential flow. Indeed, the formation of weak vortex zones (dead zones) downstream of the vertical baffles is observed, attributed to flow attachment and lower pressure in that region. These zones tend to diminish in size as the turbine rotation speed increases, as discussed.

Figure 8 displays the velocity distribution at the vertical plane for the three distinct shapes of the spherical vessel. According to this figure, it is apparent that the size of the well-mixed zones remains unaffected by the variation in baffle design (horizontal and vertical). Therefore, to delve deeper and elucidate the role of the vessel design, the velocity component curves can suffice for this purpose.

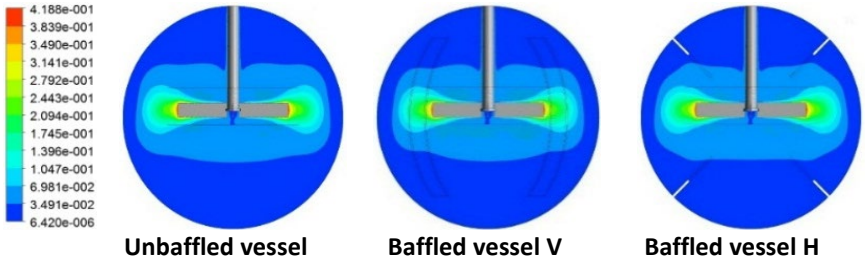

Fig. 8. Velocity contours for different vessel shapes at the agitator vertical plane

Figure 9 shows the distribution of tangential and radial velocities along two horizontal lines, one situated within the impeller plane at its blade (Figure 6.c), and the other within the same plane but above the blade (Figure 6.d). It also illustrates the axial velocity distribution along two vertical lines, one passing through the blade (Figure 6.e), and the other within the same plane but distant from the blade (Figure 6.f). The tangential velocity along line (c) remains unaffected by the installation of baffles due to the predominance of tangential flow. However, along line (d), it is relatively less significant in the case of a vessel equipped with vertical baffles. Furthermore, the velocity is relatively more substantial in the case of horizontal baffle installation near the turbine shaft. Away from this shaft, the tangential velocity is relatively higher in an unbaffled vessel. Regarding the radial velocity, along the horizontal line within the impeller plane and passing through the blade (c), there is no noteworthy alteration depending on

the baffle arrangement.

The axial velocity along the vertical lines depicted in Figures 6.e and 6.f consistently exhibits a tendency to decrease along these measurement lines, particularly with horizontal baffles. This reduction is attributed to the intensification of radial flow, leading to a decrease in axial stream. Additionally, in the case of horizontal baffles, their arrangement diminishes the axial velocity by creating an additional loop, as discussed in Figure 7.

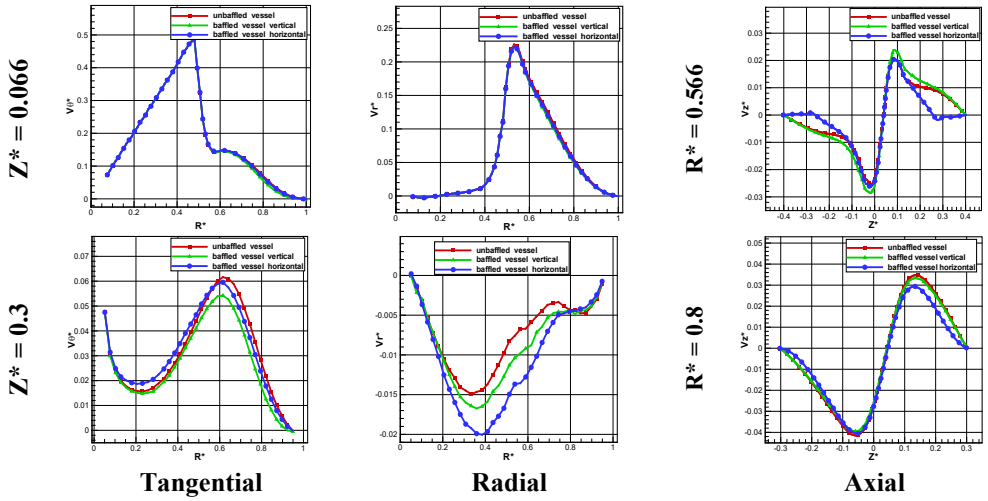

Fig. 9. Velocity components for various vessel shapes along different measurement lines

5.2 Effect of baffled number

Due to the significant influence of radial flow induced by the disk turbine in an agitated spherical vessel equipped with horizontal baffles, it has been deemed essential to maintain this geometric configuration and highlight the effect of the baffles number according to this arrangement on the hydrodynamic behavior within this vessel.

Hence, the Reynolds number and the behavior index have been set at 150 and 0.8, respectively. Figure 10 presents the variation in streamline patterns with respect to the number of horizontal baffles, specifically 4, 8, and 10. It can be observed that an increase in the number of horizontal baffles leads to a reduction in the size of the additional axial loop noted previously with the use of this type of baffle.

Moreover, the flow becomes more complex, especially in the presence of a shear-thinning fluid.

On the horizontal plane, the formation of small dead zones is noticeable in the case of 10 baffles, indicating the creation of additional loops due to the prominence of obstacles within the agitated vessel.

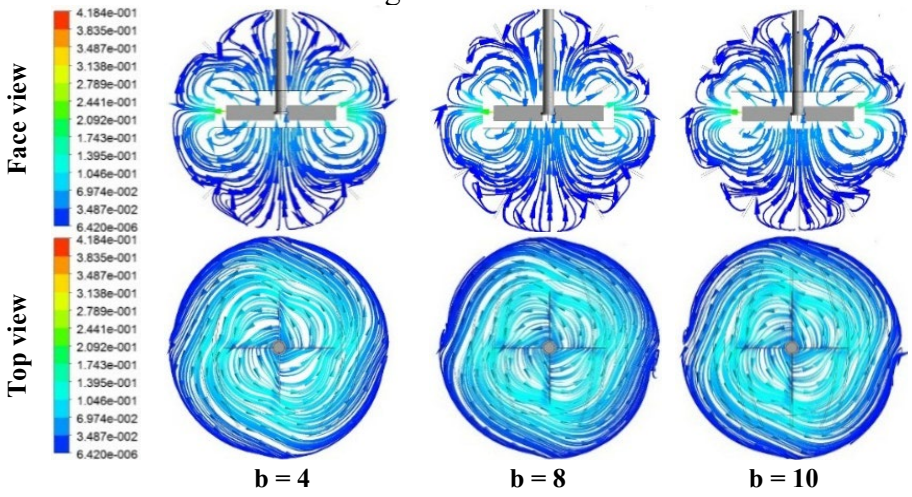

Fig. 10. Streamlines for different baffle number according to different views

Figure 11, illustrating the velocity distribution within the vertical plane as a function of the number of baffles, indicates that the well-mixed zone remains unaffected by the number of baffles near the disk turbine blades. However, due to the presence of the shear-thinning fluid, the size of caverns tends to decrease relatively with the increase in the number of horizontal baffles.

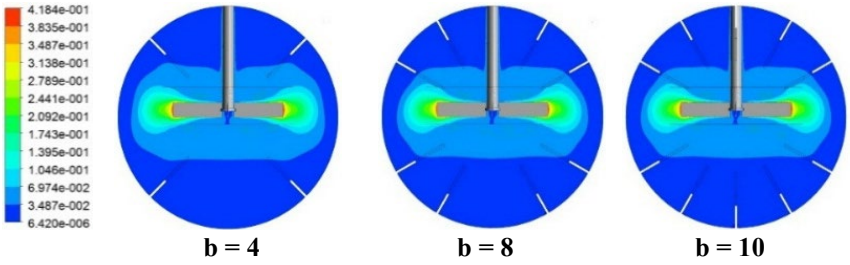

Fig. 11. Velocity contours for different baffle number at the agitator vertical plane

Figure 12 displays the tangential velocity profiles along two horizontal lines and radial profiles along two horizontal lines drawn in the impeller plane, see Figure 6.c, d. This Figure also illustrates the distribution of axial velocity along two vertical lines, see Figure 6.e and f. From this figure, it can be seen that the tangential and the radial velocities along the line (c) appear similar for all baffle number. Nevertheless, through a zoom in certain regions, it can be observed that these velocities show a slight tendency of decrease with the baffle number.

Indeed, the shape without baffles (b = 0) has a relatively high tangential and radial velocity compared with the other baffled vessels. In addition, along line (d) the tangential velocity is relatively higher in the case of a baffled vessel with b = 10 near the turbine shaft. However, away from this shaft, tangential velocity is relatively higher in an unbaffled vessel (b = 0). Moreover, along this line, the radial velocity is lower in the case of a vessel without baffles (b = 0). Furthermore, an increase in the number of baffles leads to a reduction in radial velocity near the turbine shaft. However, at a distance away from this shaft, a clear tendency to an increase in radial velocity is observed. On the other hand, near the wall, the radial velocity of the configuration without baffles is predominant. This effect is due to the presence of dead zones, which has been discussed in Figure 10. The axial velocity along the vertical lines shown in Figures 6.e and 6.f. Along the line (e), there is an increase in the axial velocity, especially pronounced with the addition of more horizontal baffles. This increase is attributed to the reduction in the size of additional axial loops, as depicted in Figure 10, Furthermore, in the present observations, the axial velocity is important near the vessel top in the case of baffled vessel due to the obstacles created by the presence of this baffles. Conversely, in the line (f), the effect is reversed. Indeed, the spherical configuration without baffles shows a significantly higher velocity compared to other configurations.

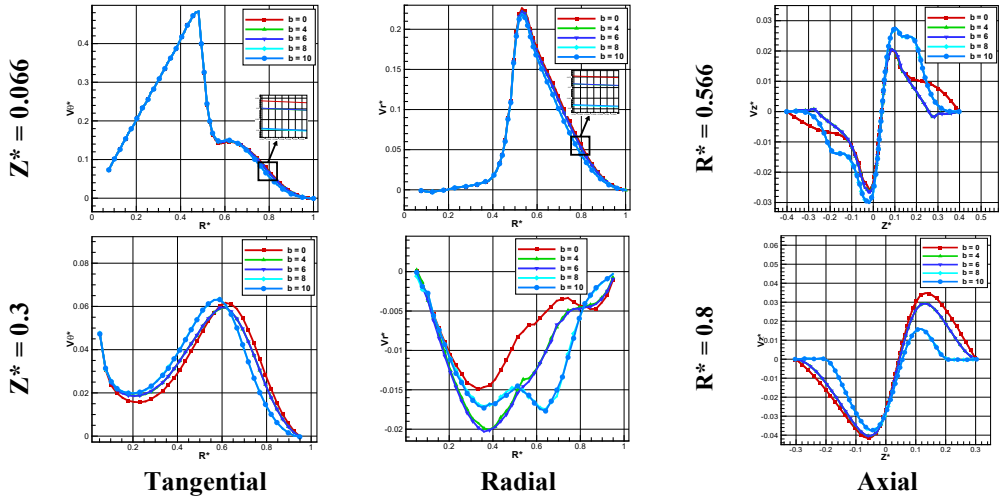

Fig. 12. Velocity components for various baffle number along different measurement lines

5.3 Power consumption

The study of mechanical agitation of a shear-thinning fluid in a tank with various baffle configurations cannot be complete without considering energy consumption. The dimensionless power number is key to optimizing energy use, considering factors like Reynolds number, baffle configuration, and the fluid's behavior index. The Reynolds number is treated as a global parameter, with power number variations shown for other parameters. Figure 13a shows the logarithmic variation of the power number with Reynolds number for different behavior indices of the shear-thinning fluid. As the Reynolds number increases and the behavior index decreases, the power number decreases, indicating reduced energy consumption due to lower local viscosity. Figure 13 illustrates power number variations for different baffle configurations (13b) and numbers of baffles (13c). Although the curves are similar across Reynolds numbers, their impact on energy behavior is better understood through tabular data.

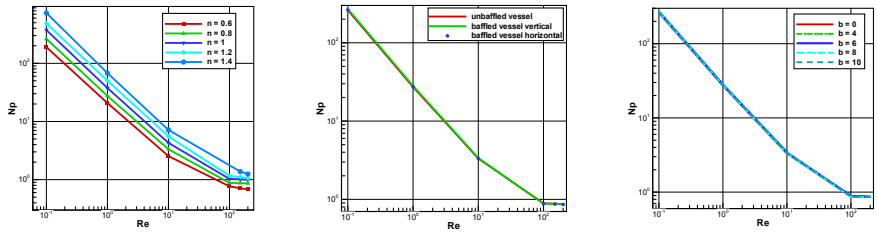

(a) behavior index **(b) Baffle disposition** **(c) Baffle number**

Fig. 13. Power number as a function of Reynolds number for different baffled vessel

Table 4 presents power numbers for low (Re = 1), moderate (Re = 10), and high (Re = 150) Reynolds numbers in baffled spherical vessels, comparing simple and baffle-equipped vessels. The power increases by approximately 3% in laminar flow with baffles, while in transitional flow, it remains nearly unchanged. Specifically, for Re = 1 and 10, vertical baffles increase power by 2.84% and 1.38%, respectively, while horizontal baffles increase power by 0.56% and 0.19%. Horizontal baffles lead to lower energy consumption due to smoother flow. Increasing the number of horizontal baffles from 4 to 10 raises energy consumption by 0.86% at Re = 10. Nevertheless, in this situation, it can be considered that the installation of baffles, although affecting the hydrodynamic behavior, does not lead to significant energy changes.

Table 4

Power number for different vessel shapes at varying Reynolds numbers

Unbaffled vessel		Baffled vessel				
		Vertical baffle	Horizontal baffle			
Baffle number	*b = 0*	*b = 4*	*b = 4*	*b = 6*	*b = 8*	*b = 10*
Re = 1	27.287	28.063	27.441	27.443	27.595	27.597
Re = 10	3.3233	3.3693	3.3299	3.3501	3.3580	3.3587
Re = 150	0.8811	0.8781	0.8701	0.8696	0.8615	0.8594

6. Conclusions

The work presented in this paper involves a numerical investigation of the hydrodynamic and energy behavior of a shear-thinning fluid in a spherical vessel stirred by a disk turbine. The impacts of disk turbine rotational speed, fluid rheology, baffle configuration, and their quantity have been highlighted on the mentioned behaviors. Consequently, the analysis of various results has revealed the following key points:

• The installation of baffles, in addition to overcoming flow disturbances on the impeller, increases radial velocity, especially in the case of a horizontal arrangement of these baffles. Nevertheless, the actual energy consumption, which should theoretically increase with the installation of baffles, remains relatively low, except for a certain upward trend, particularly in the case of vertical baffles.

• The percentage increase in energy consumption for baffled tanks compared to the standard tank (without baffles) decreases as the Reynolds number increases, with the power increase being more significant for Reynolds numbers below 10.

• For moderate Reynold number (Re=10), energy consumption rises by 1.38% with vertical baffles compared to the standard tank (without baffles), while it increases by only 0.19% with horizontal baffles.

• A reduction in energy consumption corresponds to a decrease in viscosity in well-mixed regions.

• Due to the significant impact of horizontal baffle installation on the intensification of radial flow, their quantity was examined in terms of hydrodynamics and energy consumption. Indeed, with an increase in the number of horizontal baffles, a noticeable increase in axial velocity is observed, with a minor increase in energy consumption.

• With an increase in the number of baffles, energy consumption rises by a percentage of 0.86% compared to the standard vessel. However, it can be considered unchanged because it does not even reach 1% for moderate Reynolds numbers.

It would be interesting to explore the impact of the geometry, arrangement, and size of the baffles on hydrodynamic and energy performance at higher Reynolds numbers. Future research should also focus on the practical application of these impeller designs and their impact on larger-scale applications.

REFERENCES

[1] *S. Nagata,* Mixing: Principles and Applications, Halsted Press, 1975.
[2] *N. Papastefanos, M. Stamatoudis,* Effect of impeller and vessel size on impeller power number in closed vessels for Reynolds numbers between 40 and 65000, Chemical Engineering Communications, Vol. **80**, No. 1, P. 69–79, 1989, DOI:10.1080/00986448908940516.
[3] *C. Xuereb, M. Poux, J. Bertrand,* Agitation and Mixing: Fundamental Aspects and Industrial Applications, Dunod, 2006
[4] *H. Ameur,* Agitation of yield stress fluids in different vessel shapes, Engineering Science and Technology, an International Journal, Vol. **19**, No. 1, P. 189–196, 2016, DOI:10.1016/j.jestch.2015.06.007.
[5] *C.D. Taca, M. Paunescu,* Power input in closed stirred vessels, Chemical Engineering Science, Vol. **56**, P. 4445–4450, 2001, DOI:10.1016/S0009-2509(01)00096-3.
[6] *H. Yapici, G. Basturk,* CFD modeling of conjugate heat transfer and homogeneously mixing two different fluids in a stirred and heated hemispherical vessel, Computers & Chemical Engineering, Vol. **28**, P. 2233–2244, 2004, DOI:10.1016/j.compchemeng.2004.03.008.
[7] *M.F.W. Distelhoff, A.J. Marquis,* Scalar mixing in the vicinity of two disk turbines and two pitched blade impellers, Chemical Engineering Science, Vol. **55**, No. 10, P. 1905–1920, 2000, DOI:10.1016/S0009-2509(99)00464-9.
[8] *D. Chapple, S.M. Kresta, A. Wall, A. Afacan,* The effect of impeller and tank geometry on power number for a pitched blade turbine, Chemical Engineering Research and Design, Vol. **80**, No. 4, P. 364–372, 2002, DOI:10.1205/026387602317446407.
[9] *J. Aubin, N. Le Sauze, J. Bertrand, D.F. Fletcher, C. Xuereb*, PIV measurements of flow in an aerated tank stirred by a down- and an up-pumping axial flow impeller, Experimental Thermal and Fluid Science, Vol. **28**, No. 5, P. 447–456, 2004, DOI:10.1016/j.expthermflusci.2001.12.001.
[10] *V. Boonkanokwong, R.P. Frank, P. Valliappan, B. Remy, J.G. Khinast, B.J. Glasser,* Flow of granular materials in a bladed mixer: effect of particle properties and process parameters on impeller torque and power consumption, Advanced Powder Technology, Vol. **29**, No. 11, P. 2733–2752, 2018, DOI:10.1016/j.apt.2018.07.022.
[11] *Z. Jia, L. Xu, X. Duan, Z.S. Mao, Q. Zhang, C.C. Yang,* CFD simulation of flow and mixing characteristics in a stirred tank agitated by improved disc turbines, Chinese Journal of Chemical Engineering, Vol. **50**, P. 95–107, 2022, DOI:10.1016/j.cjche.2022.05.017.
[12] *Z. Driss, G. Bouzgarrou, W. Chtourou, H. Kchaou,* Computational studies of the pitched blade turbines design effect on the stirred tank flow characteristics, European Journal of Mechanics B/Fluids, Vol. **29**, No. 3, P. 236–245, 2010, DOI:10.1016/j.euromechflu.2010.01.006.
[13] *H. Wang, X. Duan, X. Feng, Z.S. Mao, C. Yang,* Effect of impeller type and scale-up on spatial distribution of shear rate in a stirred tank, Chinese Journal of Chemical Engineering, Vol. **42**, P. 351–363, 2022, DOI:10.1016/j.cjche.2021.03.004.

[14] *S. Youcefi, A. Mokhefi, M. Bouzit,* Theoretical study of thermo-hydrodynamic performances inside an agitated tank equipped with modified two-blade design, Thermal Science and Engineering Progress, Vol. **55**, P. 102866, 2024, DOI:10.1016/j.tsep.2023.102866.

[15] *R. Zadghaffari, J.S. Moghaddas, J. Revstedt,* A mixing study in a double-Rushton stirred tank, Computers & Chemical Engineering, Vol. **33**, No. 7, P. 1240–1246, 2009, DOI:10.1016/j.compchemeng.2009.01.017.

[16] *X. Xiong, Z. Liu, C. Tao, Y. Wang, F. Cheng, H. Li,* Reduced power consumption in stirred vessel with high solid loading by equipping punched baffles, Chinese Journal of Chemical Engineering, Vol. **56**, P. 203–214, 2023, DOI:10.1016/j.cjche.2022.07.018.

[17] *S. Youcefi, M. Bouzit, H. Ameur, Y. Kamla, A. Youcefi,* Effect of some design parameters on the flow fields and power consumption in a vessel stirred by a Rushton turbine, Chemical and Process Engineering, Vol. **34**, No. 2, P. 293–307, 2013, DOI:10.2478/cpe-2013-0024.

[18] *S. Youcefi, M. Bouzit, A. Youcefi, A. Mokhefi,* Effect of an inclined slots on the power consumption and vortices size in a Rushton turbine agitated tank, Chinese Journal of Mechanical Engineering, Vol. **36**, No. 1, P. 147, 2023, DOI:10.1186/s10033-023-00981-8.

[19] *S. Roy, S. Acharya,* Scalar mixing in a turbulent stirred tank with pitched blade turbine: Role of impeller speed perturbation, Chemical Engineering Research and Design, Vol. **90**, No. 7, P. 884–898, 2012, DOI:10.1016/j.cherd.2011.10.009.

[20] *S. Youcefi, A. Youcefi,* Power consumption and mixing time in rheologically complex fluids by a two-bladed impeller, Journal of Mechanical Science and Technology, Vol. **29**, No. 2, P. 543–548, 2015, DOI:10.1007/s12206-015-0114-1.

[21] *P.A. Tanguy, G. Ascanio,* Mixing of shear-thinning fluids with dual off-centred impellers, The Canadian Journal of Chemical Engineering, Vol. **83**, No. 3, P. 393–400, 2005, DOI:10.1002/cjce.5450830301.

[22] *S. Wang, P. Wang, J. Yuan, J. Liu, Q. Si, D. Li,* Simulation Analysis of Power Consumption and Mixing Time of Pseudoplastic Non-Newtonian Fluids with a Propeller Agitator, Energies, Vol. **15**, No. 13, P. 4561, 2022, DOI:10.3390/en15134561.

[23] *A.S.M. Nekrouf, S. Youcefi, M. Bouzit,* Optimization of fluid dynamics by shear thinning in stirred tanks using anchor stirrers with convergent hollows, Journal of the Serbian Society for Computational Mechanics, Vol. **18**, No. 2, P. 77–95, 2024, DOI:10.24874/jsscm.2024.18.02.05.

[24] *H. Ameur, M. Bouzit,* Numerical investigation of flow induced by a disk turbine in unbaffled stirred tank, Acta Scientiarum. Technology, Vol. **35**, No. 3, P. 469–476, 2013.

[25] *Z. Asghar, M. W. S. Khan, A. A. Pasha, M. M. Rahman, L. Sankaralingam, M. I. Alam,* On non-Newtonian fluid flow generated via complex metachronal waves of cilia with magnetic, hall, and porous effects, Physics of Fluids, Vol. **35**, No. 9, 2023, DOI:10.1063/5.0164439.

[26] *A.S.M. Nekrouf, S. Youcefi, M. Bouzit, A. Mokhefi,* Hydrodynamic and Energetic Study of a Non-Newtonian Fluid with a Flexible and Transformable Blade Anchor, International Journal of Modern Physics C, 2025, DOI:10.1142/S0129183125500470.

[27] *A. Mokhefi, M. Bouanini, M. Elmir, P. Spitéri,* Effect of an anchor geometry on the hydrodynamic characteristics of a nanofluid in agitated tank, Defect and Diffusion Forum, Vol. **409**, P. 179–193, 2021, DOI:10.4028/www.scientific.net/DDF.409.179.

[28] *S. Youcefi, A. Mokhefi, M. Bouzit, A. Youcefi, Energy-Efficient Design Optimization of Two-Bladed Agitators in Cylindrical Tanks, International Journal of Heat & Technology, Vol. 41, No. 6, 2023, DOI:10.18280/ijht.410611*

[29] *A. Dewan, V. Buwa, F. Durst,* Performance optimizations of grid disc impellers for mixing of single-phase flows in a stirred vessel, Chemical Engineering Research and Design, Vol. **84**, No. 8, P. 691-702, 2006, DOI:10.1205/cherd05044.

[30] *H. Patil, A.K. Patel, H.J. Pant, A. Venu Vinod,* CFD simulation model for mixing tank using multiple reference frame (MRF) impeller rotation, ISH Journal of Hydraulic Engineering, Vol. **27**, No. 2, P. 200-209, 2021, DOI:10.1080/09715010.2018.1535921.
[31] *F. Moukalled, L. Mangani, M. Darwish,* The Finite Volume Method, Fluid Mechanics and Its Applications, Vol. **113**, P. 103-135, 2016, DOI:10.1007/978-3-319-16874-6_5.